ANISOTROPY-INVARIANT MAPPING OF TURBULENCE IN A SWIRLING PIPE FLOW

Mira Pashtrapanska
Department of Applied Physics
Radbound University Nijmegen
Graalburcht, 6525 ED Nijmegen, The Netherlands
M.Pashtrapanska@science.ru.nl

Jovan Jovanović
Lehrstuhl für Strömungsmechanik
Universität Erlangen-Nürnberg
Cauerstraße 4, 91058 Erlangen, Germany
jovan@lstm.uni-erlangen.de

Franz Durst
Lehrstuhl für Strömungsmechanik
Universität Erlangen-Nürnberg
Cauerstraße 4, 91058 Erlangen, Germany
durst@lstm.uni-erlangen.de

ABSTRACT

This paper reports laser-Doppler measurements of the mean flow and turbulence stresses in a swirling pipe flow. Experiments were carried out under well-controlled laboratory conditions in a refractive index-matched pipe flow facility. The results show pronounced asymmetry in mean and fluctuating quantities during the downstream decay of the swirl. Experimental data reveal that the swirl significantly modifies the anisotropy of turbulence and that it can induce explosive growth of the turbulent kinetic energy during its decay. Anisotropy invariant mapping of the turbulent stresses shows that the additional flow deformation imposed by initially strong swirling motion forces turbulence in the core region to tend towards the isotropic two-component state.

INTRODUCTION

There are numerous engineering flows in which the rotation part of the mean rate of deformation represents the major contribution. These flows include turbines, pumps, fans and cyclone separators. Owing to complex coupling between the turbulent stress, which is a symmetric tensor, and the rotation part of the mean rate of deformation, which is an antisymmetric tensor, the turbulent constitutive relations are more complex than in purely strained flows.

Swirling turbulent shear flows, such as decaying swirl flow in a straight pipe, were studied experimentally by Baker (1967), Fejer et al. (1968), Wolf et al. (1969), Murakami et al. (1976), Kitoh (1991), Li and Tomita (1994), Steenbergen (1995) and Rocklage-Marliani et al. (2003). These investigations showed that depending on the initial velocity distribution, the swirl decay can undergo completely different scenarios with regions which can stabilize or destabilize turbulence causing the flow field to be fairly complex. Experience gained from the analysis of swirling flows leads to the conclusion that these flows cannot be successfully predicted with the standard two-equation model of turbulence. To predict turbulence in swirling flows successfully, a Reynolds stress model of turbulence is required.

The objective of this paper is to present new experimental data on the mean velocity and second-order turbulence statistics in turbulent swirling pipe flow using the laser-Doppler technique. The purpose of the experiments was to establish detailed information on the influence of swirl on the anisotropy of turbulence. According to the Taylor-Proudman theorem, which states that in a rapidly rotating frame fluctuating velocity components will be restricted to the planes normal to the rotation axis (Speziale, 1998), we expect that initially strong swirl will decrease the anisotropy to a minimum and that the anisotropy will increase during the swirl decay towards the state of maximum anisotropy, which is the chief peculiarity of turbulence in simple wall-bounded flows (see also Fig. 7). By measuring the components of the Reynolds stress tensor during the swirl decay, it is therefore possible to study the influence of the anisotropy of turbulence on the dynamics of the turbulent kinetic energy, inter-component energy transfer and the turbulent dissipation rate.

TEST SECTION AND MEASURING TECHNIQUE

The experimental investigations were carried out in the refractive index matched pipe flow facility at the Lehrstuhl für Strömungsmechanik in Erlangen using LDA. This general-purpose test ring allows high spatial resolution laser-Doppler measurements of the mean velocity field and the turbulence statistics at low and moderate Reynolds numbers.

Test section and swirl generator

The experimental facility , shown schematically in Fig. 1, was described in detail by Durst et al. (1995).

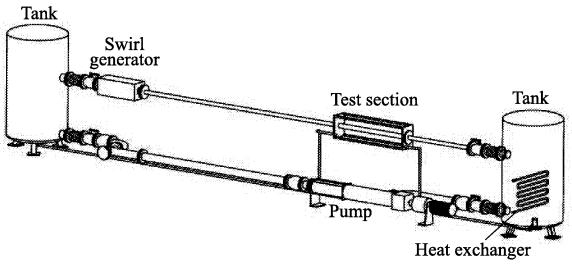

Figure 1: Sketch of the experimental setup.

It is a closed-loop pipe flow installation driven by a screw conveyer pump operating in suction mode. The diameter D and the length L of the pipe were 50 mm and about 7 m, respectively. In order to impose additional deformation on the basic flow, a swirl generator was installed at the inlet of the pipe. as shown in Fig. 1. It consisted of a rotating housing which was 50 mm in inner diameter and 0.5 m in length and a honeycomb formed out of small tubes of 4 mm outer diameter. At the pipe entrance the circumferential velocity distribution imposed on the flow by the rotating honeycomb was nearly linear across the pipe radius. The swirl generator was driven by a three-phase alternating motor controlled by a frequency converter which allowed adjustment of the rotation rate of up to 1130 r.p.m. Figure 2 shows the swirl generator and the front view of the honeycomb.

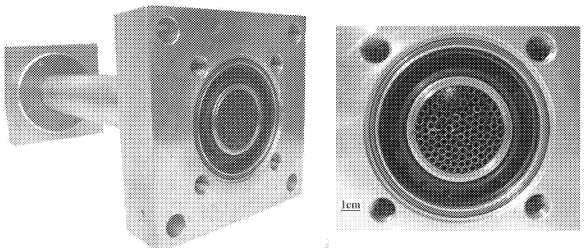

Figure 2: The swirl generator and the honeycomb.

In oder to permit laser-Doppler measurements, the pipe test section was made from Duran-50 glass and mounted in a viewing box, which was filled with the working fluid. To avoid any possible interference of the laser beams with the pipe walls, the working fluid was selected to be refractive index-matched to the Duran glass.

The experiments without swirl were first carried out at the maximum flow rate corresponding to the Reynolds number, based on a pipe diameter D and the bulk velocity U_B, of Re $\simeq 30{\times}10^3$. The measurements in a swirling pipe flow were performed at a number of measuring stations L/D = 3, 10, 17.3, 37.3, 44.8, 52.3, 81.7, 98.4 downstream of the pipe inlet. A "strong" swirl was generated, at the maximum flow rate, by setting the outer circumferential velocity of the swirl generator to U_B (N = 1).

Measuring technique

A specially designed laser-Doppler system was used for the present measurements. This system and its arrangement with respect to the test section are shown schematically in Fig. 3.

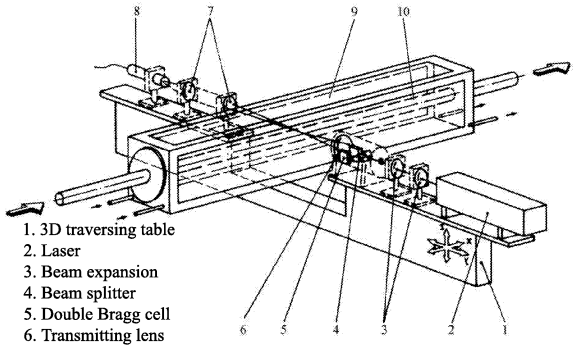

Figure 3: The LDA system and the test section.

The optical system consisted of a 15 mW He-Ne laser, collimator for adjustment of the beam waist, Bragg cells for resolving the flow direction, the transmitting and receiving lenses and avalanche photodiode. Further details of the laser-Doppler system employed can be found in Durst et al. (1995).

The LDA system was operated in the forward scattering mode. The scattered light from the particles was detected by an avalanche photodiode. The signals from this diode were further processed using a TSI Model 1990 counter processor. At each measuring position at least N = 20000 independent samples were taken. For this size of sample the relative statistical uncertainty in the measurements, on the basis of the sampling parameters, was estimated to be about $\pm 0.5\%$ for the mean velocity and $\pm 1.5\%$ for the second-order moments.

By assuming that the flow is axially symmetric about the pipe axes, the one-component LDA system permitted measurements of the mean flow field and all components of the Reynolds stress tensor. In order to accomplish such measurements, the LDA optical system was mounted at different angles α with respect to the pipe axis and profiles were taken along horizontal ($\beta = 0°$), vertical ($\beta = 90°$) and inclined ($\beta = \pm 45°$) directions.

TURBULENT PIPE FLOW WITHOUT SWIRL

In order to prove reliability of the test section and of the laser-Doppler technique for turbulence measurements and to demonstrate the great potential of the analytical tools available for interpretation of the dynamics of turbulence, we shall consider first turbulent pipe flow without swirl.

Mean flow

The measured mean velocity profile, as a function of the normalized distance from the wall $r' = R - r$, is shown in Fig. 4. The coordinates $r = 0$ and $r = R$ in the radial direction correspond to the pipe centerline and the pipe wall, respectively. Normalization of the measurements was performed with respect to inner wall variables defined as $r'^{+} = r' u_\tau/\nu$ and $\overline{U}_x^{+} = \overline{U}_x/u_\tau$ where u_τ is the wall shear velocity $u_\tau = (\tau_w/\rho)^{1/2}$, τ_w is the wall shear stress $\tau_w = \mu(d\overline{U}_x/dr')_{wall}$ and ρ, μ and ν are density and dynamic and kinematic viscosity of the working fluid, respectively. The wall shear stress τ_w was calculated from the slope of the measured velocity profile in the viscous sublayer.

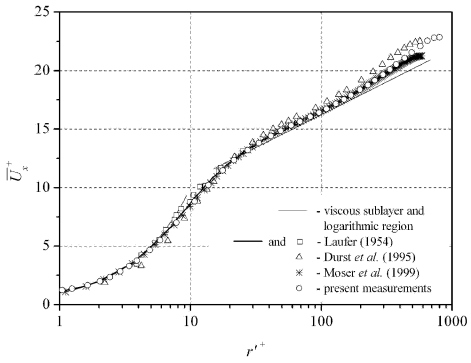

Figure 4: Mean velocity distribution for $\mathrm{Re} = 30 \times 10^3$.

The measured mean flow distribution shown in Fig. 4 closely follows the universal law of the wall: the linear and the logarithmic portions of the normalized velocity profile can be easily identified. The data from Fig. 4 show very good agreement with our previous measurements reported by Durst et al. (1995), experimental results of Laufer (1954) and the mean velocity distribution deduced from numerical simulations of Moser et al. (1999).

Turbulence intensity measurments

Turbulence intensity measurements of axial ($u_x^{'} = \sqrt{\overline{u_x^2}}$), radial ($u_r^{'} = \sqrt{\overline{u_r^2}}$) and tangential ($u_\theta^{'} = \sqrt{\overline{u_\theta^2}}$) velocity fluctuations normalized with the wall shear velocity are shown in Fig. 5. These results are presented versus the distance from the wall normalized with the pipe radius. The new set of experimental data compare well with previous measurements by Durst et al. (1995) and also with those reported by Laufer (1954).

Figure 6 shows comparison between the calculated turbulent shear stress $\overline{u_x u_r}$ obtained from the mean velocity data using the momentum equation and by direct measurements. The achieved degree of agreement is excellent.

We may use results presented in Figs. 5 and 6 to study variations of the anisotropy of turbulence in a pipe flow. Such analysis provides very useful insights relevant for easy and transparent understanding the dynamics of turbulence in thin shear flows.

Following the analysis of Lumley and Newman (1977), the level of anisotropy of turbulence can be quantified using the anisotropy tensor

$$a_{ij} = \frac{\overline{u_i u_j}}{q^2} - \frac{1}{3}\delta_{ij} \tag{1}$$

and its scalar invariants

$$\mathrm{II}_a = a_{ij}a_{ji} \tag{2}$$

$$\mathrm{III}_a = a_{ij}a_{jk}a_{ki} \tag{3}$$

In principal axes each component of a_{ij} cannot be smaller than $-1/3$ and not larger than $2/3$. Lumley (1978) concluded from these restrictions that all realizable turbulence must lie inside the region bounded by the joint variations of II_a and III_a in axisymmetric turbulence

$$\mathrm{II}_a = \frac{3}{2}\left(\frac{4}{3}|\mathrm{III}_a|\right)^{2/3} \tag{4}$$

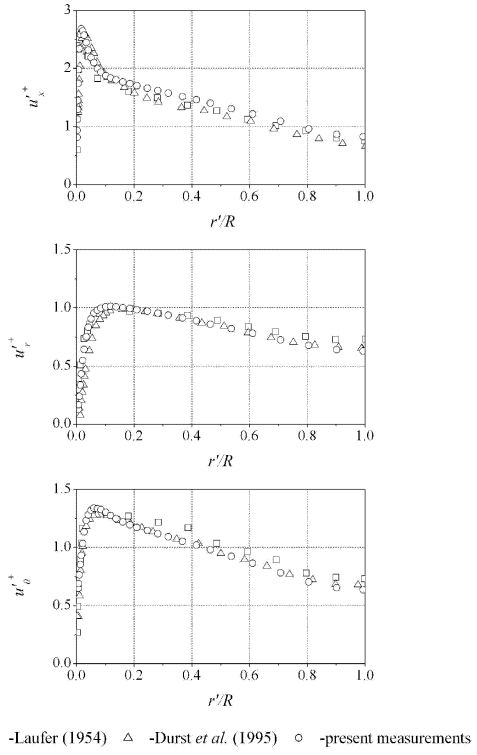

Figure 5: Turbulence intensities of the velocity fluctuations: (a) axial velocity component; (b) radial velocity component; (c) tangential velocity component.

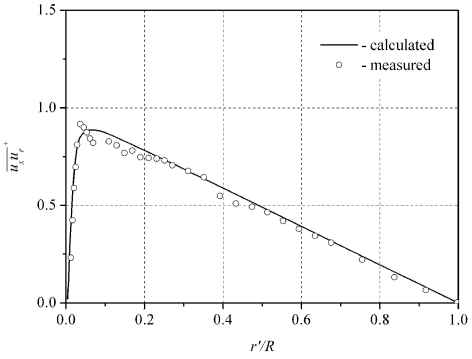

Figure 6: Comparison between the measured and calculated turbulent shear stress.

and two-component turbulence:

$$\mathrm{II}_a = \frac{2}{9} + 2\mathrm{III}_a \tag{5}$$

Figure 7 shows the plot of (4) and (5), which defines the anisotropy-invariant map and bounds all realistic turbulence. Both curves shown in this figure correspond to axisymmetric turbulence and the straight line represent two-component turbulence. The limiting states of the turbulence are located at the corner points on the right- and left-hand sides of the anisotropy-invariant map and correspond to the one-

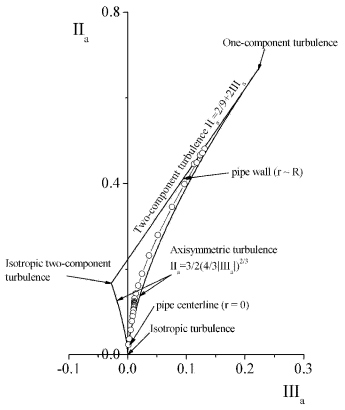

Figure 7: Anisotropy-invariant map and the trace of the joint variation of II_a and III_a for turbulent pipe flow.

component state and the isotropic two-component state, respectively.

It is useful to examine the trajectory of the joint variation of the invariants II_a and III_a across the anisotropy-invariant map for pipe flow since it can shed considerable light on our capability to interpret the dynamics of turbulence in thin shear layers. Figure 7 reveals that in a pipe flow, the anisotropy lies close to the two-component state and the axisymmetric state. In the region of the viscous sublayer ($r'^+ < 5$), the data closely follow the two-component state. Starting from the wall ($r'^+ = 0$), the anisotropy first increases towards the right corner point of the anisotropy-invariant map which corresponds to the one-component state. At the edge of the viscous sublayer ($r'^+ \simeq 8$), the invariants reach their maximum values and thereafter follow closely the right boundary of the map, which characterizes axisymmetric turbulence. At the pipe centerline, the anisotropy nearly vanishes, indicating a tendency towards isotropy.

TURBULENT PIPE FLOW WITH SWIRL

In this section we present experimental results that correspond to the downstream development of initially strong N = 1 swirl in pipe flow. The experimental data include measurements of the mean velocity components and terms of the Reynolds stress tensor. These data are normalized with the bulk velocity U_m calculated from the volume flow rate and the cross-sectional area of the pipe. The evolution of the swirl decay is analyzed by looking at profiles measured in radial planes at different measuring stations downstream from the swirl generator, the location of which is defined as L/D = 0.

Downstream decay of an initially strong swirl

For an initially strong swirl, the decay process starts with symmetric velocity distributions as indicated in Fig. 8. This figure shows that the profiles of axial and tangential velocity components in the region L/D = 3 – 17.3 exhibit nearly perfect symmetry with respect to the pipe centerline. Profiles of the radial velocity component confirm that it is negligible and plays no important role in the evolution of the swirl decay.

In the region between L/D = 3 and L/D =17.3, the vortex core can be distinguished by linear variation of the tangential velocity component with the radial distance from the pipe centerline (see marked details in Fig. 8). Within the flow

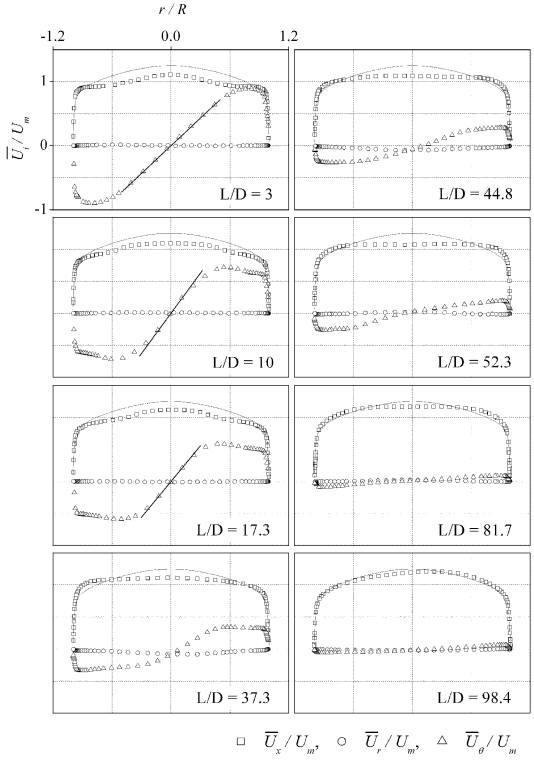

Figure 8: Normalized mean velocity distributions in a swirling pipe flow for an initially strong swirl. Note that the scales on the vertical axis are same for all presented data and that dashed curves represent swirl-free pipe flow data.

region occupied by the vortex core, the rate of rotation remains constant. Owing to the action of viscosity, which forces the flow near the solid surface to satisfy non-slip boundary conditions, the initially linear trend in the profiles of the tangential velocity component disappears rapidly as the swirl decays downstream. The gradient of the tangential velocity component increases within the vortex core as the swirl decays downstream. The region of the vortex core extends about 60% of the pipe radius at L/D = 3 and this structure is preserved at L/D = 17.3 across a narrower region accounting for about 30% of the pipe radius. This evidence suggests that, under the present experimental conditions, the vortex core persisted in the region L/D < 30 and was completely dissolved at downstream measuring locations.

Measured mean velocity distributions imply that nonexistence of the vortex core in the flow region L/D $\geq$ 30 produces asymmetric decay of the swirl and causes difficulties in interpretation of the measured results. Asymmetry is pronounced in profiles of the tangential velocity component especially close to the pipe walls where large differences can be noticed for r/R = 1 and r/R = -1. Note that at L/D = 37.3 asymmetry is associated with a gentle increase in the radial velocity component. Asymmetry is less evident in distributions of the axial velocity component which display local maxima away from the pipe centerline. Far from the swirl generator large differences exist between the center of swirl and the position of maximum velocity. This difference persisted in the measured data even at L/D = 98.4 and suggest that it

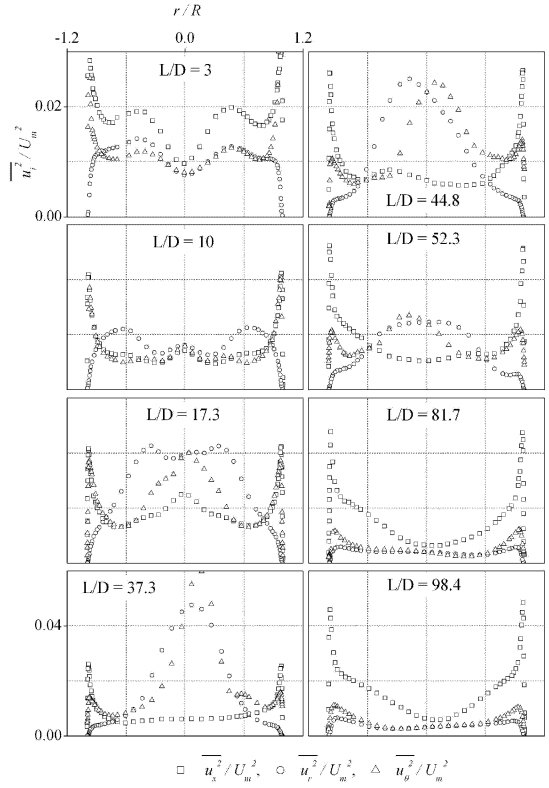

Figure 9: Normalized distributions of diagonal components of the Reynolds stress tensor in a swirling pipe flow for an initially strong swirl.

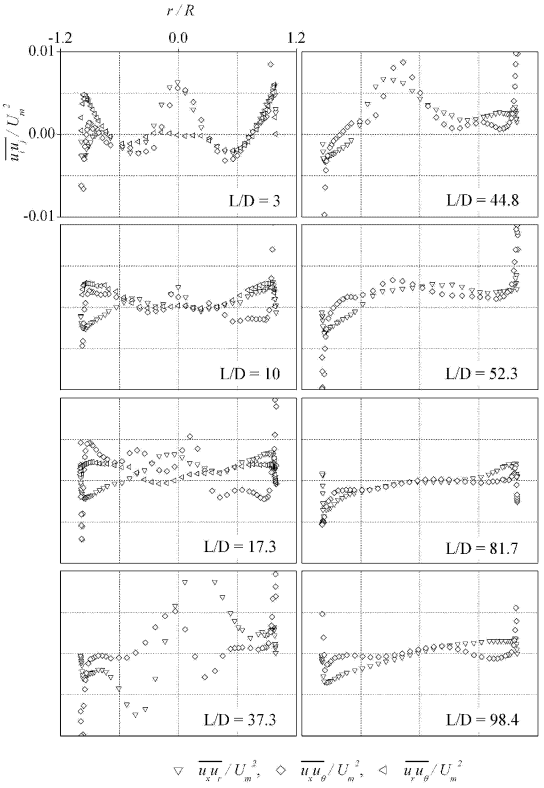

Figure 10: Normalized distributions of off-diagonal components of the Reynolds stress tensor in a swirling pipe flow for an initially strong swirl.

would vanish only if the swirl is completely dissolved into a fully developed pipe flow.

The evolution of turbulence intensities during the swirl decay are shown in Fig. 9. The initial development of the normal turbulent stresses is symmetric with respect to the pipe centerline and the symmetry is preserved over the entire region where the vortex core could be identified in the experimental data of the mean velocity field.

From the first measuring station corresponding to L/D = 3, all intensity components decay slowly up to the next station L/D = 10 where they reach a turbulence level of about 10%. At L/D = 17.3, the anisotropy of turbulence around the pipe centerline changes character from $\overline{u_x^2} > \overline{u_r^2} \simeq \overline{u_\theta^2}$ ($\mathrm{III}_a \geq 0$), to $\overline{u_x^2} < \overline{u_r^2} \simeq \overline{u_\theta^2}$ ($\mathrm{III}_a \leq 0$) which is followed by explosive growth of the turbulent kinetic energy and subsequent breakdown of the flow symmetry. Measured intensity profiles reveal that the observed change in the turbulence anisotropy is associated with an increase in the radial and the tangential stresses which overweigh the axial stress around the pipe centerline.

Downstream from L/D = 17.3, the turbulent intensities develop in an asymmetric fashion towards a fully developed flow condition. Asymmetry, which is preserved during late states of the swirl decay, is pronounced mainly near the pipe centerline and to a lesser extent near pipe walls. Turbulence intensities at the pipe centerline reach a maximum level at L/D = 37.3 with the peak value exceeding 30%. From this measuring station, turbulence intensities and the anisotropy in the core region slowly decay downstream and approach values, at L/D = 98.4, which are typical for fully developed pipe flow without swirl.

Turbulent shear stress measurements are presented in Fig. 10. Owing to breakdown in flow symmetry downstream from L/D > 17.3, it was not possible to determine $\overline{u_r u_\theta}$ during the later stages of the swirl decay and corresponding data are missing in Fig. 10. The initial development of the shear stresses, in the region where the vortex core exists, L/D = 3 – 17.3, is symmetric about $r = 0$, but turbulence is not axisymmetric along the pipe centerline since not all of the shear stress components are zero there. Inspection of equations for the mean flow under reflection of the radial coordinate suggest that such a situation prevents the symmetric flow development. Nearly perfect symmetry in the profiles of the mean flow and turbulent intensities close to the swirl generator imply that the flow is strongly influenced by the initial conditions.

Breakdown of the flow symmetry and explosive growth of the turbulent energy downstream from L/D > 17.3 are also reflected in measured distributions of the shear stress components. These distributions are highly asymmetric and a few times larger in magnitude than in a fully developed pipe flow. As the swirl intensity decays, the distributions of the shear stresses reduce in amplitude and approach regular forms far downstream. Profiles taken at L/D = 81.7 and 98.4 display the trend to restore the flow symmetry and axisymmetry of turbulence at the pipe centerline during the final stages of the swirl decay.

Anisotropy-invariant mapping, shown in Fig. 11, provides

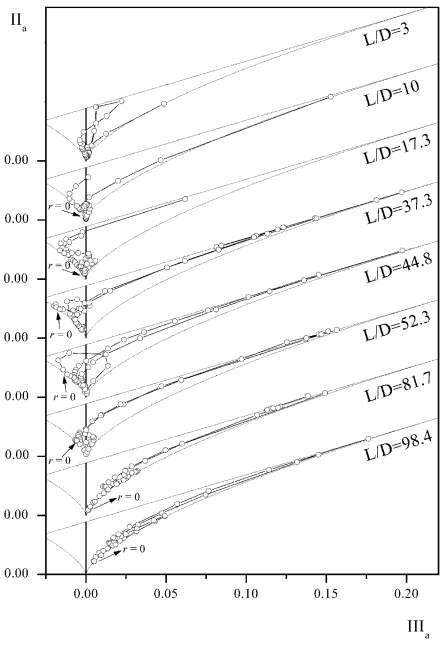

Figure 11: Anisotropy-invariant mapping of turbulence in a swirling pipe flow for an initially strong swirl. Note that the data very close to the wall are located at the line representing the two-component state of turbulence.

additional insights relevant for an improved understanding of the dynamics of turbulence initialized by strong swirl. In the region close to the swirl generator L/D= 3 – 17.3 the anisotropy lies close to the left boundary of the anisotropy-invariant map. At these measuring stations, turbulence develops in the presence of the vortex core and tend towards the isotropic two-component state. In the light of the Taylor-Proudman theorem, such a tendency in the data is not surprising. The qualitative analysis of the dissipation rate equation leads to the conjecture that for such turbulence, which appears in the anisotropy map close to the isotropic two-component limit, there will be explosive production of turbulence energy until the anisotropy relaxes towards the trajectory common for fully developed pipe flow. The experimentally observed influence of the swirl on the turbulence anisotropy is in agreement with results obtained by Oerlue et al. (2004) and very similar to that found by the direct numerical simulations by Orlandi and Fatica (1997) and Eggels et al. (1994).

As the swirl decays downstream, the anisotropy gradually increases along the two-component state. As the flow approaches the fully developed state, the anisotropy shifts from the left-hand boundary towards the right-hand boundary of the anisotropy-invariant map. Hence, during the swirl decay turbulence covers large portions of the anisotropy map and reaches nearly all limiting states of turbulence. At the last measuring station L/D = 98.4, the anisotropy settles very close to the typical pattern of the fully developed flow as shown in Fig. 7.

Acknowledgments

This research received financial support from the Deutsche Forschungsgemeinschaft (Grant Jo 240/3-2). We gratefully acknowledge this support. The authors wish to thank Profs. P. Bradshaw and H. Nagib for continuous support and numerous discussions during their stay at the Lehrstuhl für Strömungsmechanik in Erlangen. We gratefully acknowledge the advice and support received from Prof. V. Vasanta Ram, who provided the swirl generator for the experimental setup.

REFERENCES

Baker, D.W., 1967, "Decay of swirling, turbulent flow of incompressible fluids in long pipes", PhD thesis, University of Maryland.

Durst, F., Jovanović, J. and Sender, J., 1995, "LDA measurements in the near-wall region of a turbulent pipe flow", *J. Fluid Mech.*, Vol. 295, pp. 305-335.

Eggels, J.G.M., Boersma, B.J. and Nieuwstadt, F.T.M., 1994, "Direct and large-eddy simulations of turbulent flow in an axially rotating pipe", Sumitted to *J. Fluid Mech.*

Fejer, A., Lavan, Z. and Wolf, L., 1968, "Study of swirling fluid flows", ARL 68-0173, Aeroscale Research Laboratories.

Kitoh, O., 1991, "Experimental study of turbulent swirling flow in a straight pipe", *J. Fluid Mech.*, Vol. 225, pp. 445-479.

Laufer, J., 1954, "The structure of turbulence in fully developed pipe flow", NACA TN 1174.

Li, H. and Tomita, Y., 1994, "Characteristics of swirling flow in a circular pipe", *J. Fluids Eng.*, Vol. 116, pp. 370-373.

Lumley, J.L. and Newman, G.R., 1977, "The return to isotropy of homogeneous turbulence", *J. Fluid Mech.*, Vol. 82, pp. 161-178.

Lumley, J.L., 1978, "Computational modeling of turbulent flows", *Adv. Appl. Mech.*, Vol. 18, pp. 123-176.

Moser, R.D., Kim, J. and Mansour, N.N., 1999, "DNS of turbulent channel flow up to Re_τ=590", *Phys. Fluids*, Vol. 11, pp. 943-945.

Murakami, M., Kito, O., Katayama, Y. and Iida, Y., 1976, "An experimental study of swirling flow in pipes", *Bull. JSME*, Vol. 19, pp. 118-126.

Oerlue, R., Micheel, J. and Vasanta Ram, V., 2004, "Characteristics of the turbulent fluctuating motion in swirling flow", *Advances in Turbulence X*, CIMNE, Barcelona, Spain, pp. 872.

Orlandi, P. and Fatica, M., 1997, "Direct simulations of a turbulent pipe rotating along the axis", *J. Fluid Mech.*, Vol. 343, pp. 43-72.

Rocklage-Marliani, G., Schmidts, M. and Vasanta Ram, V.I., 2003, "Three-dimensional laser-Doppler velocimeter measurements in swirling turbulent pipe flow", *Flow, Turbulence and Combustion*, Vol. 70, pp. 43-67.

Speziale, C.G., 1998, "A review of material frame-indifference in mechanics", *Appl. Mech. Rev.*, Vol. 51, pp. 489-504.

Steenbergen, W., 1995, "Turbulent pipe flow with swirl", PhD thesis, University of Eindhoven.

Wolf, L., Lavan, Z. and Fejer, A., 1969, "Measurements of the decay of swirl in turbulent flow", *AIAA Journal*, Vol. 7, pp. 971-973.